NANO LETTERS

2008
Vol. 8, No. 4
1020-1025

Linear Electrooptic Coefficient of InP Nanowires

Clint J. Novotny,[†] Christopher T. DeRose,[‡] Robert A. Norwood,[‡] and Paul K. L. Yu*,[†]

Department of Electrical and Computer Engineering, University of California—San Diego, La Jolla, California 92093, and College of Optical Sciences, University of Arizona, Tuscon, Arizona 85721

Received October 18, 2007; Revised Manuscript Received January 30, 2008

ABSTRACT

A novel fabrication procedure is developed that allows for the direct measurement of the linear electrooptic coefficient of semiconducting nanowires to determine their viability for use in electrooptic devices. Vertically aligned InP nanowires are transferred from their growth substrate to a glass substrate using a host polymer, while still retaining the alignment of the nanowires. The linear electrooptic coefficient of the InP nanowires exhibited a 1−2 orders of magnitude enhancement over bulk InP and ranged from 31 to 147 pm/V. The figure of merit, n^3r, exhibited a factor of 20 enhancement over lithium niobate and ranged from 1010 to 4817 pm/V.

Semiconductor nanowires (NWs) have gained a lot of attention over the past decade due to their unique geometry and properties. Studies have been conducted to gain a more in-depth understanding of the basic properties of the NWs and how they compare to bulk material. Mechanical,[1,2] thermal,[3] electrical transport,[4–6] optical,[7,8] phonon,[9] and magnetic[10,11] properties have all been investigated. However, to the best of our knowledge, there has been no study performed that directly measures the electrooptic properties of NWs. The goal of this paper is to design an experiment that can directly measure the electrooptic coefficient of InP NWs and determine the possibility of their use in devices such as electrooptic modulators.

In order to accurately measure the electrooptic coefficient tensor components, one must be able to relate the application of an electric field to the material's crystal lattice. For the case of a poled polymer, the electric field is typically applied along the z-axis of the polymer.[12,13] In order to measure the coefficient of the NWs, they must all have the same crystal orientation. The chosen orientation of the NWs in this experiment is perpendicular to the substrate. A structure is designed that removes the nanowires from their growth substrate using a host polymer while keeping the vertical alignment of the NWs intact. To the best of our knowledge, this is the first structure that has allowed the direct measurement of the electrooptic coefficient of nanowires.

The measurement of the electrooptic coefficient is based on a technique developed by Teng and Man[14] by using the setup depicted in Figure 1. A laser with wavelength 1.31 μm is incident on the backside of the glass substrate at an angle of 45° with its polarization at 45° to the incident plane. The light passes through a transparent electrode, indium tin oxide (ITO), to the polymer/NW matrix and reflects off a gold electrode. It is assumed that there is no absorption in the polymer layer because the wavelength used is above the bandgap of the NWs. The light then exits the sample and passes through a Babinet-Soleil compensator that is used to control the relative retardation between the perpendicular (s wave) and parallel (p wave) components of the optical field from 0 to 2π. After the compensator, the beam passes through an analyzer crossed against the incoming polarization and then to the detector. The continuous wave intensity of the reflected beam at the detector is given by[14]

$$I = I_{\max} \sin^2\left(\frac{\varphi^{sp}}{2}\right) \tag{1}$$

where $I_{\max}$ is the maximum intensity and φ^{sp} is the phase retardation between the s and p waves. When a modulating voltage (~1 kHz), $V = V_m \sin(\omega_m t)$, is applied to the ITO and Au contacts, a change in the phase angle of the s and p waves is induced by the change in refractive index due to the electrooptic effect. The modulated intensity, I_m, should increase linearly with the applied voltage, V_m, due to the linear electrooptic effect.

III−V semiconductors, such as InP, belong to the zinc blende group with crystal symmetry $\bar{4}3m$.[15] The electrooptic tensor for this group is[16]

* Corresponding author. E-mail: yu@ece.ucsd.edu.
† University of California—San Diego.
‡ University of Arizona.

10.1021/nl072688k CCC: $40.75
Published on Web 03/01/2008

$$r_{ij} = \begin{pmatrix} 0 & 0 & 0 \\ 0 & 0 & 0 \\ 0 & 0 & 0 \\ r_{41} & 0 & 0 \\ 0 & r_{41} & 0 \\ 0 & 0 & r_{41} \end{pmatrix} \quad (2)$$

When an electric field, E, is applied, a birefringence is induced and the initially spherical index ellipsoid distorts to[16]

$$\frac{x^2+y^2+z^2}{n^2} + 2r_{41}(E_x yz + E_y xz + E_z xy) = 1 \quad (3)$$

where n is the static index of refraction and x, y, and z are parallel to the crystallographic axes [100], [010], and [001], respectively. The nanowires in this study have an orientation of [111] and therefore the electric field in this configuration will be applied in the [111] direction. Equation 3 then becomes

$$\frac{x^2+y^2+z^2}{n^2} + \frac{2r_{41}E_0}{\sqrt{3}}(yz + xz + xy) = 1 \quad (4)$$

where

$$\vec{E} = \frac{E_0}{\sqrt{3}}(\hat{x} + \hat{y} + \hat{z})$$

By transforming the coordinate system such that the new z-axis lies in the [111] direction, the ellipsoid equation leads to the following indices

$$n_x' = n_y' \cong n + \frac{n^3 r_{41} E_0}{2\sqrt{3}} \quad (5a)$$

$$n_z' \cong n - \frac{n^3 r_{41} E_0}{\sqrt{3}} \quad (5b)$$

The phase retardation, φ^{sp}, between the s and p waves is given by[17]

$$\varphi^{sp} = \frac{4\pi d}{\lambda}[n_e(\theta_e)\cos\theta_e - n_o \cos\theta_o] \quad (6)$$

where $\theta_{e,o}$ refers to the internal angle in the slab of the extraordinary and ordinary waves, respectively, λ is the wavelength of the incident laser light, and d is the thickness of the slab of material. By using simple geometrical considerations (Snell's law) and substituting eqs 5a and 5b for the indices, an expression for $d\varphi^{sp}/dV$ can be reached (where $E_0 = V/d$):

$$\frac{d\varphi^{sp}}{dV} = \frac{6\pi}{\lambda\sqrt{3}} \frac{n_{eff}^2 \sin^2\theta}{\sqrt{n_{eff}^2 - \sin^2\theta}} r_{41} \quad (7)$$

where n_{eff} is the effective index of the composite layer, θ is the angle of incidence, and r_{41} is the linear electrooptic coefficient of the polymer/NW composite. This derivation considers only the polymer/glass-ITO interface and the polymer/gold interface with the assumption that multiple reflections do not occur. In order to obtain values for r_{41}, $d\varphi^{sp}/dV$ must be related to experimentally obtainable quantities. Differentiating eq (1) and normalizing by I_{max} leads to the relationship

$$\frac{1}{I_{max}}\frac{dI_m}{dV} = \frac{\sin\varphi^{comp}}{2}\frac{d\varphi^{sp}}{dV} \quad (8)$$

During the experiment, the compensator (φ^{comp}) is set such that $\sin(\varphi) = 1$ and dI_m/dV can be approximated by I_m/V_m (experimentally measured values of the modulated intensity at the detector, I_m, and the applied modulating voltage, V_m). Thus, the linear electrooptic coefficient of the NW/polymer composite system is given by

$$r_{41} = \frac{\lambda\sqrt{3}}{3\pi} \frac{\sqrt{n_{eff}^2 - \sin^2\theta}}{n_{eff}^2 \sin^2\theta} \frac{1}{I_{max}} \frac{I_m}{V_m} \quad (9)$$

The effective index of refraction is derived by extending the Maxwell−Garnett theory[18] for the case of cylindrical particles

$$n_{eff} = n_{polymer} \sqrt{\frac{(1-FF)\left(\frac{1}{2} + \frac{n_{InP}^2}{2n_{polymer}^2}\right) + \frac{n_{InP}^2}{n_{polymer}^2}FF}{(1-FF)\left(\frac{1}{2} + \frac{n_{InP}^2}{2n_{polymer}^2}\right) + FF}} \quad (10)$$

where the fill factor, FF, is defined as the ratio of the volume of the InP NWs to the volume of the polymer layer. It is important to note that the raw data will provide the coefficient for the composite system. The NW electrooptic coefficient is determined by dividing eq 9 by each sample's fill factor.

InP NWs are grown on InP(111)B substrates in a horizontal MOCVD reactor at a pressure of 100 Torr. Trimethylindium (TMIn) and phosphine (PH_3) are used as the group III and V sources, respectively, with hydrogen as the carrier gas. The substrates are annealed at 600 °C under PH_3 for 10 min and then cooled down to the growth temperature of 425 °C. The input V/III ratio for all samples is 190, while the growth time varies from sample to sample. NW characterization was carried out using a Phillips XL30 environmental scanning electron microscope (SEM), operating at 20 kV. The polymer used in this experiment is poly(methyl methacrylate) (PMMA). PMMA is typically used in polymer-based systems as a passive, host material due to its excellent optical properties, reasonably high thermal stability, and good processability; it has a negligible electrooptic coefficient.[19,20]

Vertically aligned InP NWs are grown without the use of a deposited metal catalyst. Indium droplets form on the surface to create nucleation sites for NW growth. The details of this process can be found elsewhere.[21] This process creates NWs with very uniform diameter and length. The average and standard deviation values of the NW dimensions for each growth used in this experiment can be found in Table 1. A control sample, labeled Ref1, consisting of PMMA only was used for comparison purposes.

Besides consistent vertical alignment of the NWs, another requirement for this measurement is the removal of the nanowires from their host InP substrate. Because the substrate and NWs are the same material, they have the same crystal orientation with respect to the electric field as well as the same index of refraction. It would therefore be difficult to differentiate between the effects of the substrate and NWs on the value of the coefficient. To remove any ambiguity, a fabrication scheme has been devised that removes the NWs

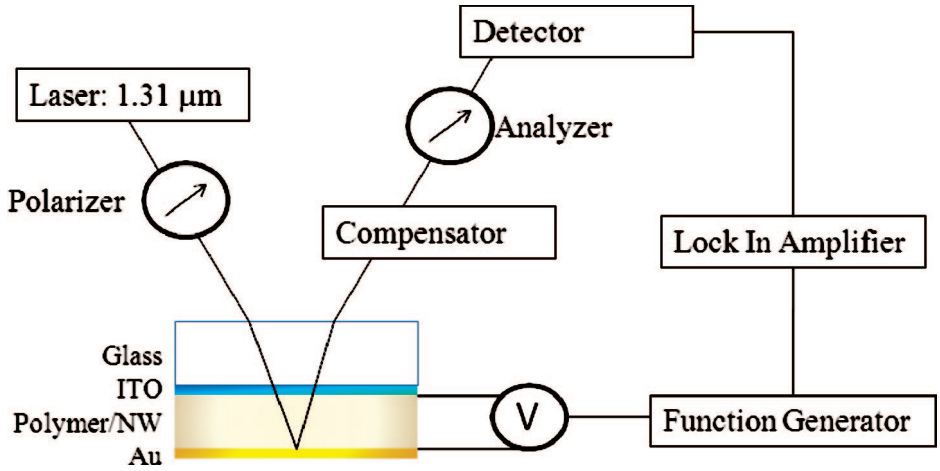

Figure 1. Experimental setup for electrooptic coefficient measurement.

Table 1. Average and Standard Deviation Values for the Thickness of the PMMA Layer, h, and for the Diameter (d), Length (L), and Density (D) of the NW Samples[a]

sample	h (nm)	L (nm)	d (nm)	D (NWs/cm^2)	fill factor	r_{eff} (pm/V)	r_{NW} (pm/V)	n^3r_{NW} (pm/V)
Ref1	1320 ± 100				0%	0		
InP610a	880 ± 100	553 ± 118	26.7 ±1.9	$2.7 \times 10^9 \pm 8.0*10^8$	0.83%	1.2	147	4817
InP610b	880 ± 100	559 ± 123	24.0 ± 1.8	$3.4 \times 10^9 \pm 8.6*10^8$	0.85%	1.1	131	4279
InP611a	1100 ± 100	700 ± 165	50.9 ± 2.4	$3.8 \times 10^9 \pm 4.8*10^8$	4.50%	4.4	97	3175
InP611b	1320 ± 100	886 ± 178	43.9 ± 2.1	$3.6 \times 10^9 \pm 9.3*10^8$	3.47%	1.1	31	1010
InP613b	1320 ± 100	878 ± 153	32.0 ± 2.6	$4.2 \times 10^9 \pm 6.1*10^8$	2.11%	0.8	37	1227
bulk InP							1.5	50
$LiNbO_3$							$r_{33} = 34.1$ $r_{13} = 10.3$	$n_e^3r_{33} - n_o^3r_{13}$ $= 222$

[a] The electrooptic coefficient of the hybrid system, r_{eff}, is given along with the calculated values for the NW electrooptic coefficient, r_{NW}, and the figure of merit, n^3r. A comparison to bulk InP[24] and $LiNbO_3$[25,26] is provided.

from their growth substrate and embeds them in PMMA while retaining their necessary vertical alignment.

The entire fabrication process is depicted in Figure 2. ITO (50 nm) is sputtered onto a glass substrate using a Denton Discovery 18 Sputter System. The resistivity of this ITO layer is 6.8×10^{-4} Ω cm, as determined by four point probe measurements. A 165 nm layer of silicon dioxide (SiO_2) is then deposited at 350 °C using an Oxford Plasmalab PECVD. This layer provides protection for the ITO during etching. Finally, an adhesion promoter, hexamethyldisilazane (HMDS), is spun-cast onto the SiO_2, followed by a deposition of 110 nm of PMMA.

Multiple spins of PMMA diluted in anisole (~100 nm/spin) are cast onto the NW sample until the desired thickness is achieved. This dilution is necessary because 100% PMMA is too viscous and shear flattens the NWs during spin-casting. Thicknesses of ~100 nm/spin retain the necessary vertical alignment of the NWs. Typically the final PMMA thickness is ~200 nm taller than the maximum NW height of each sample to ensure full encapsulation of the NWs. The next step is to remove the large edge beads present after spin-casting. Because the edge beads are typically 10 times the thickness of the layer, the samples will only bond at the edges, missing all the NWs in the middle of the sample. Edge-bead removal is accomplished by oxygen plasma etching using a Trion RIE/ICP dry etcher. After the edge-bead removal, the samples are ready to be bonded.

The NW sample and glass substrate are brought together on a hot plate at 190 °C. After 10 min, pressure is then applied to the samples to facilitate PMMA to PMMA bonding. The hot plate temperature is then lowered to 150 °C for 1 h to allow for reflow and enhancement of acid resistance of the bond layer. The samples are placed into undiluted hydrochloric acid (HCl) heated to approximately 80 °C. In this step, the etch chemistry of InP plays an important role. HCl will strongly etch the (100), (110), and (111)B surfaces of InP. However, the (111)A surface etches at a much slower rate. Unlike the (111)B surface which has two spare electrons per atom, the (111)A surface has no spare electrons and is therefore much less reactive than (111)B.[22] Studies have shown that the (111)A surface etches 30 times slower in HCl than the (111)B surface.[23] In this setup, the [111]B direction points downward toward the glass substrate with the [111]A direction exposed to the acid. Thus, the substrate is etched from the edges. Once the substrate is removed, the acid only accesses the [111]A surface of the NWs and therefore they will not etch. Figure 3 depicts a sample before and after the substrate has been removed and the host PMMA has been etched. Before processing, the sample has vertically aligned NWs. During processing, some

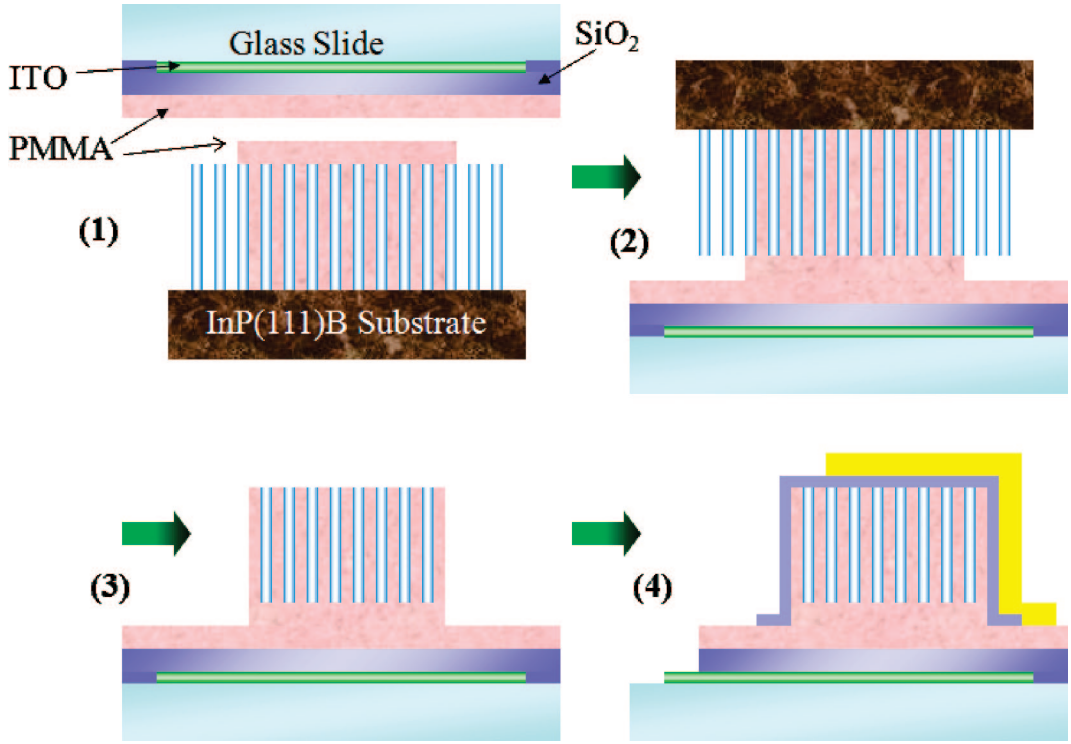

Figure 2. Test structure fabrication process. (1) Coat host glass substrate with 50 nm of ITO, 165 nm of SiO_2, and 110 nm of PMMA. Coat NW sample with PMMA and remove edge beads. (2) Bond two substrates together. (3) Etch off InP substrate in HCl. (4) Open ITO window by etching PMMA and ITO. Cover bonded layer with SiO_2 and Au.

of the PMMA has been completely etched while other areas of the PMMA are only slightly etched and remain after the O_2 dry etch due to hard baking. Because some of the PMMA has been removed, an examination of the NWs inside this layer is possible. Protruding NWs are seen in Figure 3b, providing proof that the fabrication process does not etch the NWs and also that the NWs retain their crucial vertical alignment.

Once the substrate is etched, a thin layer (30 nm) of SiO_2 is sputtered onto the bonded NW layer to prevent the Au contact from touching the NWs. While Figure 3b depicts NWs protruding from the PMMA layer, the actual bonding process does not have a PMMA dry etch step and therefore the NWs will not protrude as seen in Figure 3b, allowing the SiO_2 to fully cover the NWs. Next, a window is opened to access the ITO electrode. This is accomplished by covering most of the sample with a glass slide while exposing only a small section of it to dry etching. The PMMA layer is dry etched in O_2 and the SiO_2 layer is dry etched in SF_6. The final step is to deposit a gold layer on top of the structure that acts as both an electrode and a reflective surface for the incoming light. The final structure is shown in Figure 4.

The response of each sample (intensity measured at the detector) to the applied modulating voltage is shown in Figure 5. As expected, the control PMMA sample (labeled Ref1) has no measurable increase with the applied voltage. The NW samples, on the other hand, show a pronounced linear electrooptic effect from the applied voltage. These experimental data, along with eq 9 and the fill factor for each sample are used to determine the electrooptic coefficient of each NW sample. Table 1 summarizes the results of this

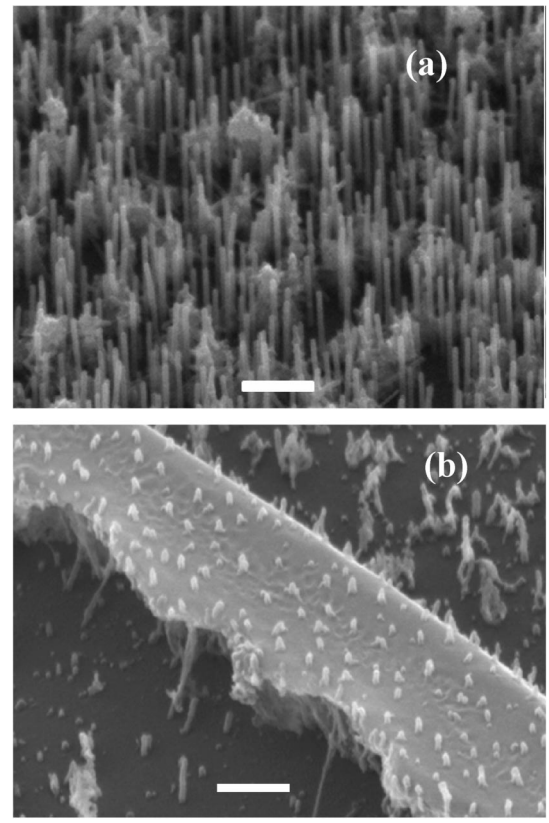

Figure 3. SEM images taken at a 45° tilt of (a) NW sample before processing and (b) NW/PMMA sample after substrate removal of O_2 etch, showing the NWs survive the substrate etch and remain vertical. The scale bar for both images is 500 nm.

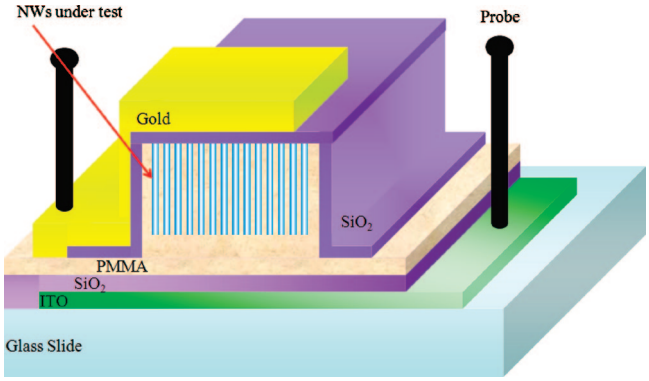

Figure 4. Final test structure for measurement of the NW electrooptic coefficient.

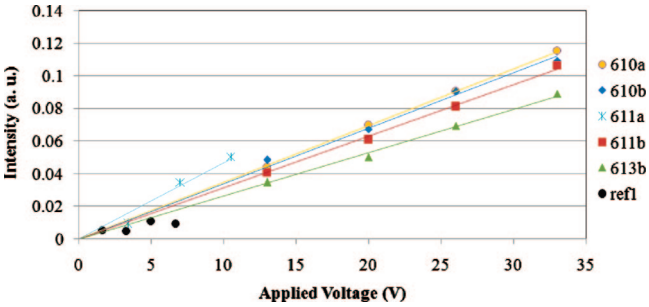

Figure 5. Measurement results showing the response of each sample to the applied modulating voltage.

analysis for all samples along with a comparison to bulk InP and $LiNbO_3$. r_{eff} is calculated for each applied modulating voltage, and the average value is shown in Table 1. Data for sample InP611a as well as the PMMA control sample were taken only at low modulating voltages. At higher applied voltage, these samples broke down. The reasons for this breakdown are unclear at the present time and require further experimentation. The PMMA, however, is not poled, and because it is an amorphous polymer, it will have inversion symmetry and thus a negligible linear electrooptic contribution.[16]

The measured electrooptic coefficient of the PMMA/NW hybrid system ranges from 0.8 to 4.4 pm/V. A slab of bulk InP has an electrooptic coefficient of 1.5 pm/V.[24] By replacing 1% of the host polymer's volume (which by itself has no response to the modulating voltage) with InP NWs, the hybrid material now has almost the same response as an entire slab of InP. The extracted NW electrooptic coefficient values range from 31 to 147 pm/V and therefore show a 1 to 2 orders of magnitude enhancement over bulk InP. It is important to note that unlike most polymer systems, no poling voltage is required to achieve these large values for the electrooptic coefficient and the NW alignment should not degrade over time, as is often the case for poled polymers.

In order to compare these values with other material systems, it is insightful to look at a figure of merit that includes both the electrooptic coefficient and the material's index of refraction. A figure of merit typically used for electrooptic materials is the product of the cube of the index of refraction and the electrooptic coefficient, n^3r. A useful material for comparison is an industry standard electrooptic material, lithium niobate, with $n^3r \approx 222$ pm/V.[25,26] The calculated range of NW values is $n^3r \sim 1010$–4817 pm/V. Therefore, InP NWs provide a figure of merit between 5 and 20 times larger than that of one of the highest electrooptic materials used in industry. Because of growth limitations, we were not able to achieve a high loading density of the NWs in PMMA (such as 20 or 30%). However, this experiment focused on the measurement of the electrooptic coefficient and not how to get the best device performance of a NW/polymer hybrid system. In order to fully utilize the high NW electrooptic coefficient in future applications, new methods will need to be developed to create a highly filled NW/polymer composite, such as those being explored with other nanomaterials.[27]

For any nanostructured material, as the material dimensions decrease the two most important effects that influence the material's properties are quantum confinement effects and the interfacial/surface effects. In this electrooptic experiment, both the diameter of the NWs and the surface play an important role in the results. First, there is weak confinement in the NW structures. As the NW diameter decreases toward the Bohr radius (~10 nm for InP), excitons are confined to a smaller area. Thus, the electron and hole wave functions have more overlap, leading to an increase in oscillator strength.[28,29] This will enhance the electrooptic effect in the NW material. Studies performed on quantum dots have shown an increase of 1 to 2 orders of magnitude in the linear electrooptic coefficient when compared to bulk material due to the quantum confinement effect.[30,31] The largest values obtained in this study for the NW electrooptic coefficient occurred for samples with the smallest diameter. Because of some growth limitations, however, it was not possible to achieve samples with diameters at or below the Bohr radius consistently. Further experimentation is needed to provide a more complete picture of the quantum effect on NWs with diameters of 10 nm and smaller.

Second, the NWs have a very large surface area to volume ratio. They are surrounded by a material (PMMA) with a much lower dielectric constant in this experiment. This combination results in a strong electric charge interaction between the two materials, resulting in an electric dipole layer at the surface that is sometimes referred to as the dielectric confinement effect, or surface polarization. Studies have shown that this effect can accelerate the separation of excited charges and thus enhances the electric field inside the nanomaterial.[32] Furthermore, previous studies have also shown that the photoluminescence intensity for InP NWs is very anisotropic.[33] Therefore, when an electric field is applied to these NWs, the surface dipole will be extremely polarizable and very responsive to the application of that field. Because of the large surface area to volume ratio, this effect can dominate the behavior of the NW response and lead to a large enhancement of the electrooptic effect when compared to bulk. In this experiment, the effects of the fill factor (and hence the surface area) and NW diameter could not be decoupled due to growth limitations. Future experiments are

needed to isolate each effect. First, NW samples with one diameter and varying fill factors will provide insight as to how the overall surface area affects the electrooptic properties. The highest fill factor achieved in this study was 4.5%. It would be insightful to include higher fill factors to observe any screening effects that may occur at high NW concentrations. Second, samples with a single fill factor and varying diameters would provide insight into the extent of quantum confinement effects.

In conclusion, we have designed and fabricated a unique structure to measure the electrooptic coefficient of InP NWs. The bonding technique presented in this study can be used to transfer aligned NWs from their growth substrate to a new host substrate. They can then be monolithically integrated with many different types of devices. Calculated values for the electrooptic coefficient of InP NWs show an increase of 1 to 2 orders of magnitude compared to bulk InP. The highest figure of merit, n^3r, for InP NWs is a factor of 20 larger than $LiNbO_3$. We therefore believe this material to be an excellent candidate for electrooptic devices such as EO modulators.

Acknowledgment. This work was supported by the National Science Foundation under Program Nos. ECS0307247 and ECS0403589; the work at the University of Arizona was supported by the National Science Foundation's MDITR Science and Technology Center.

References

(1) Wong, E. W.; Sheehan, P. E.; Lieber, C. M. *Science* **1997**, *277*, 1971.
(2) Wu, B.; Heidelberg, A.; Boland, J. J. *Nat. Mater.* **2005**, *4*, 525.
(3) Wu, Y.; Yang, P. *Adv. Mater.* **2001**, *13*, 520.
(4) Chung, S. W.; Yu, J. Y.; Heath, J. R *Appl. Phys. Lett.* **2000**, *76*, 2068.
(5) Duan, X.; Huang, Y.; Cui, Y.; Wang, J.; Lieber, C. M. *Nature* **2001**, *409*, 66.
(6) Zhong, Z.; Qian, F.; Wang, D.; Lieber, C. M. *Nano. Lett.* **2003**, *3*, 343.
(7) Johnson, J. C.; Yan, H.; Yang, P.; Saykally, R. J. *J. Phys. Chem. B* **2003**, *107*, 8816.
(8) Johnson, J. C.; Choi, H. J.; Knutsen, K. P.; Schaller, R. D.; Yang, P.; Saykally, R. J. *Nat. Mater.* **2002**, *1*, 106.
(9) Li, D.; Wu, Y.; Kim, P.; Shi, L.; Yang, P.; Majumdar, A. *Appl. Phys. Lett.* **2003**, *83*, 2934.
(10) Beck, G.; Petrikowski, K.; Khan, H. R. *Proceedings of the Microstructure Analysis in Materials Science*, Freiberg, June 15–17, 2005.
(11) Sokolov, A.; Sabirianov, I. F.; Tsymbal, E. Y.; Doudin, B.; Li, X. Z. *J. Appl. Phys.* **2003**, *93*, 7029.
(12) Schildkraut, J. S. *Appl. Opt.* **1990**, *29*, 2839.
(13) Chollet, P. A.; Gadret, G.; Kajzar, F.; Raimond, P. *Thin Solid Films* **1994**, *242*, 132.
(14) Teng, C. C.; Man, H. T. *Appl. Phys. Lett.* **1990**, *56*, 1734.
(15) Adachi, S. *Handbook on Physical Properties of Semiconductors*; Kluwer Academic Publishers: Boston, 2004.
(16) Yariv, A. *Quantum Electronics*; Wiley and Sons: New York, 1989.
(17) Khanarian, G.; Sounik, J.; Allen, D.; Shu, S. F.; Walton, C.; Goldberg, H.; Stamatoff, J. B *J. Opt. Soc. Am. B* **1996**, *13*, 1927.
(18) Landau, L. D.; Lifshitz, E. M. *Electrodynamics of Continuous Media*; Pergamon Press: Oxford, NY, 1980.
(19) Enami, Y.; DeRose, C. T.; Mathine, D.; Loychik, C.; Greenlee, C.; Norwood, R. A.; Kim, T. D.; Luo, J.; Tian, Y.; Jen, A. K. Y.; Peyghambarian, N. *Nat. Photonics* **2007**, *1*, 180.
(20) Shi, Y.; Lin, W.; Olsen, D. J.; Bechtel, J. H.; Zhang, H.; Steier, W. H.; Zhang, C.; Dalton, L. R *Appl. Phys. Lett.* **2000**, *77*, 1.
(21) Novotny, C. J.; Yu, P. K. L. *Appl. Phys. Lett.* **2005**, *87*, 203111.
(22) Pearsall, T. P. *Properties, Processing and Applications of Indium Phosphide*; INSPEC, the Institution of Electrical Engineers: London, 2000.
(23) Tuck, B.; Baker, A. J. *J. Mater. Sci.* **1973**, *8*, 1559.
(24) Suzuki, N.; Tada, K *Jpn. J. Appl. Phys* **1984**, *23*, 291.
(25) Holmes, R. J.; Kim, Y. S.; Brandle, C. D.; Smyth, D. M. *Ferroelectrics* **1983**, *51*, 41.
(26) Boyd, G. D.; Bond, W. L.; Cater, H. L *J. Appl. Phys.* **1967**, *38*, 1941.
(27) Tay, S.; Thomas, J.; Momeni, B.; Askari, M.; Adibi, A.; Hotchkiss, P. J.; Jones, S. C.; Marder, S. R.; Norwood, R. A.; N. Peyghambarian, N *Appl. Phys. Lett.* **2007**, *91*, 221109.
(28) Huang, M. H.; Mao, S.; Feick, H.; Yan, H.; Wu, Y.; Kind, H.; Weber, E.; Russo, R.; Yang, P. *Science* **2001**, *292*, 1897.
(29) Kayanuma, Y. *Phys. Rev. B* **1988**, *38*, 9797.
(30) Ghosh, S.; Lenihan, A. S.; Dutt, M. V. G.; Qasaimeh, O.; Steel, D. G.; Bhattacharya, P. *J. Vac. Sci. Technol. B* **2001**, *19*, 1455.
(31) Zhang, F.; Zhang, L.; Wang, Y. X.; Claus, R. *Appl. Opt.* **2005**, *44*, 3969.
(32) Wu, X.; Wang, R.; Zou, B.; Wu, P.; Wang, L.; Xu, J *Appl. Phys. Lett.* **1997**, *71*, 2097.
(33) Wang, J.; Gudiksen, M. S.; Duan, X.; Cui, Y.; Lieber, C. M. *Science* **2001**, *293*, 1455.

NL072688K